Appl Phys B (2011) 105:269–276
DOI 10.1007/s00340-011-4548-6

Applied Physics B
Lasers and Optics

Experimental study of an actively mode-locked fiber ring laser based on in-fiber amplitude modulation

M. Bello-Jiménez · C. Cuadrado-Laborde · A. Diez · J.L. Cruz · M.V. Andrés

Received: 28 December 2010 / Revised version: 10 March 2011 / Published online: 13 May 2011

Abstract We report an experimental study of an actively mode-locked fiber ring laser based on the development of an efficient in-fiber amplitude modulator. Intermodal coupling induced by standing flexural acoustic waves permits the implementation of broad bandwidth (1.5 nm), high modulation depth (72%), low-insertion-loss (0.75 dB), in-fiber amplitude modulators, operating in the MHz frequency range. The experimental characterization of the laser as a function of the radio frequency voltage that controls the modulator, the length of the active fiber, and the optical bandwidth of an intracavity filter implemented with a fiber Bragg grating has led to an improved performance of the Erbium-doped fiber laser: optical pulses of 34-ps temporal width, 1.4-W peak power, and 4.75-MHz repetition rate.

M. Bello-Jiménez (✉) · A. Diez · J.L. Cruz · M.V. Andrés
Departamento de Física Aplicada y Electromagnetismo, ICMUV, Universidad de Valencia, C/ Dr. Moliner 50, Burjassot 46100, Valencia, Spain
e-mail: miguel.bello@uv.es
Fax: +34-96-3543146

A. Diez
e-mail: antonio.diez@uv.es

J.L. Cruz
e-mail: jose.l.cruz@uv.es

M.V. Andrés
e-mail: miguel.andres@uv.es

C. Cuadrado-Laborde
CONICET, P.O. Box 3, Gonnet 1897, Buenos Aires, Argentina
e-mail: christian.cuadrado@uv.es
Fax: +54-221-4712771

1 Introduction

Mode-locked fiber lasers are an essential technology to generate high-quality optical pulses at high repetition rates. In passive mode-locking schemes, the repetition rate is determined by the cavity round-trip time; therefore, synchronization to an external clock signal is not possible. On the contrary, active mode-locking operation results in a more stable operation, since each optical pulse is triggered by the modulator, which in turn can be accurately synchronized to an external clock signal. However, the main disadvantage in the active schemes is the relatively long pulse width generation in comparison to passive schemes, which can still be used to operate in the femtosecond regime.

Most of the approaches in actively mode-locked lasers rely on the use of bulk components. Unfortunately, their use highly increases the cavity losses, degrading the performance of the laser and giving rise also to etalon formation that can frustrate the mode-locking operation. In addition, they require fine alignment and good mechanical stability. It is also true that fiber-pigtailed packaged electrooptics and acoustooptics modulators have been developed later, with lower insertion losses, but still remaining relatively high as compared with in-fiber solutions. Strictly all-fiber arrangements can reduce the intracavity losses associated with coupling to bulk components; at the same time they provide inherent mechanical stability and high peak power damage, in addition to compactness and low maintenance requirements. Besides this, taking into account the strong influence that dispersion has on the mode-locking process, optical fibers are particularly well suited to form the cavity of a mode-locked laser, because the dispersion of the cavity becomes easily adjusted just by using fibers with different group velocity dispersions.

Up to date, many researchers have attempted various schemes to achieve active mode-locking operation in all-fiber lasers [1–6]. Among them, we have recently reported an actively mode-locked all-fiber ring laser using a low-insertion-loss acousto-optic modulation technique, which was based on the intermodal coupling induced by standing flexural acoustic waves in a standard optical fiber [6]. This novel type of in-fiber mode-locker provides a high amplitude modulation depth that can be used to perform active mode-locking. Now, our purpose is to show the behavior of this laser under different configurations, not only to gain physical insight into the dynamics of these kinds of lasers, but also looking toward an improvement of its performance. As a result of our experimental study, a mode-locked train of light pulses were obtained of 34-ps temporal width and 1.4-W peak power, at a repetition rate of 4.75 MHz. As compared with our previous result (95-ps pulse width and 21-mW peak power) [6], this represents a significant improvement. Further, these values are within the best results reported in the framework of actively mode-locked all-fiber lasers and demonstrate that further improvements can be reached by following this research line.

In the following Sect. 2, we start with an experimental study of the in-fiber acousto-optic modulator. Then, in Sect. 3 we describe the dependence of the pulse's parameters as a function of the applied voltage to the piezoelectric (which controls the acousto-optic modulator), the erbium-doped fiber length, and the optical bandwidth of an intracavity filter performed with an FBG; see Sects. 3.1 to 3.3, respectively. Finally, our conclusions are shown in Sect. 4.

2 The intermodal coupling acousto-optic modulator

A schematic view of the acousto-optic modulator (AOM) is shown in Fig. 1. The AOM consists of an RF source, a piezoelectric disk (PD), an aluminum concentrator horn, and a standard optical fiber uncoated, in order to prevent the attenuation of the acoustic wave. The PD is excited by the RF source to produce an acoustic flexural wave that is transmitted to the fiber by the aluminum horn. The horn is attached to the PD, and it focuses the vibration into the fiber through its tip, which is glued to the uncoated optical fiber. In order to allow the generation of a standing flexural acoustic wave, the uncoated fiber is firmly clamped at one extreme, whereas in the other it was damped.

When a flexural acoustic wave propagates along the uncoated optical fiber, it produces a periodical perturbation of the refractive index. As a result, it produces intermodal coupling between the fundamental core mode and some specific cladding modes [7, 8]. This acousto-optic interaction can be seen as the dynamic counterpart of a conventional long-period grating (LPG). Thus, the transmission properties of the acoustically induced LPG can be controlled

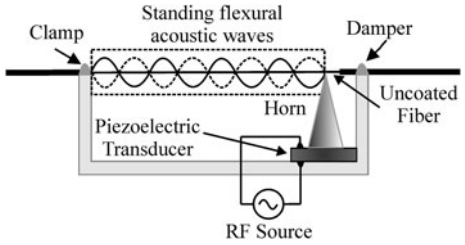

Fig. 1 Experimental setup of the acousto-optic amplitude modulator

dynamically by varying the characteristics of the flexural acoustic wave. The optical coupling is resonant in wavelength, and it takes place at the optical wavelength that verifies the phase-matching condition. At the output, only the light that remains guided by the core mode is transmitted, and the coupling between the fundamental core mode to one of the cladding modes results in the appearance of an attenuation notch in the spectrum, whose amplitude remains fixed whenever a travelling acoustic wave is used. In our experiments, the standing acoustic wave produces a modulation of the transmittance at twice the frequency of the acoustic wave.

Figure 2(a) shows the wavelength dependence of the maximum and minimum transmittance for a RF signal applied to the piezoelectric of 2.37315 MHz and 18 V (whenever we refer to voltages, it is a peak-to-peak measurement). The spectral response reveals a minimum transmittance of 9 dB at 1550.8 nm. At this wavelength the coupling between the core mode LP_{01} and the cladding mode LP_{12} produces the maximum transfer of energy [8, 9]. The period of the acoustically induced LPG is estimated to be 690 μm, obtained from the dispersion relation for a flexural wave on a cylindrical rod $\Lambda = (\pi R C_{\text{ext}} f_a^{-1})^{1/2}$ [8], where Λ is the acoustic wavelength, R is the radius the cylindrical rod, C_{ext} is the speed of the extensional wave, 5760 ms^{-1} for silica, and f_a is the acoustic wave frequency. Figure 2(b) shows the transmitted light as a function of time at the resonant optical wavelength, for the same conditions described in Fig. 2(a). An amplitude modulation can be clearly observed at 4.75 MHz, which is two times the acoustic frequency used (2.37315 MHz). The measurements reported in Fig. 2 were performed by illuminating the AOM with a laser tuned to a wavelength around the optical resonant wavelength and detecting the transmitted light in a standard oscilloscope. The fact that the reflection coefficient for the acoustic wave is not 1, makes the maximum transmission to be slightly below the reference level, i.e., the transmission of the fiber when no acoustic wave propagates. Therefore, the maximum transmission determines the insertion loss of the AOM at a given wavelength, RF frequency, and voltage. The difference between the maximum transmission and the minimum determines the modulation depth. From the results presented in Fig. 2 we can emphasize that a strong modulation depth (72%) is achieved, together with a low insertion

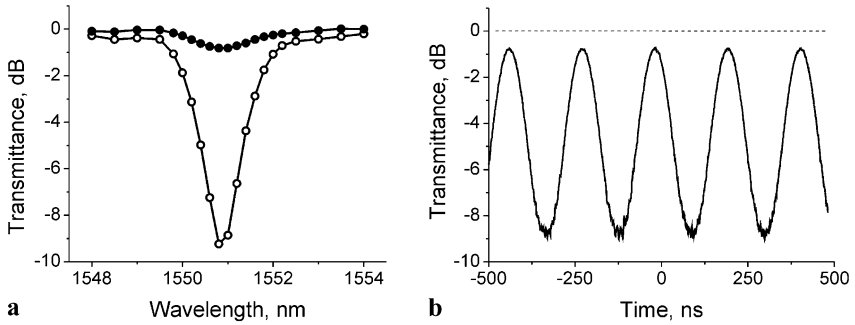

Fig. 2 (**a**) Maximum (*solid points*) and minimum (*open points*) transmittance of the AOM as a function of wavelength, around the resonance located at 1550.8 nm. (**b**) Oscilloscope trace that corresponds to the transmission of the AOM (*solid curve*) recorded at the resonant wavelength; the reference level is the *dashed line*. In both cases, $f_a = 2.37315$ MHz and $V_{PD} = 18$ V

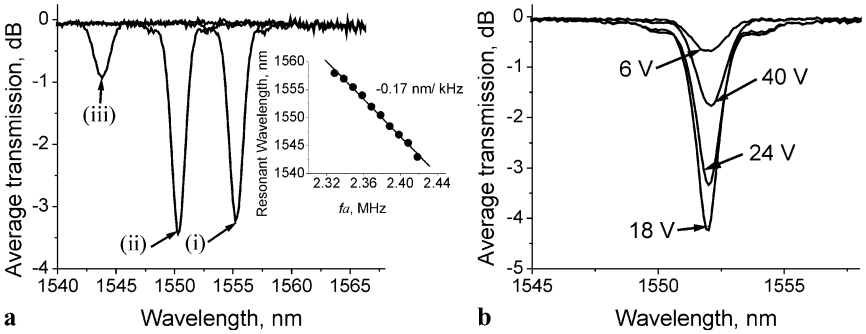

Fig. 3 (**a**) Transmission spectra at constant RF voltage (18 V) and three different acoustic frequencies: (*i*) 2.3317, (*ii*) 2.3717, and (*iii*) 2.4117 MHz. The *inset* gives the calibration of the device: Resonant wavelength versus acoustic frequency. (**b**) Transmission spectra at constant acoustic frequency (2.3731 MHz) and four different RF voltages (see the label of each trace)

loss (0.75 dB) and a broad operation bandwidth (1.5 nm). If we compare the values of these three parameters with the values recently reported for an AOM based on longitudinal acoustic waves in a FBG [5] (15% modulation depth, 1-dB insertion loss, and 6-pm bandwidth), then we can appreciate the improvement achieved with the present AOM.

The modulator has a number of specific characteristics that require to be properly analyzed. On the one hand, we have measured the operation of the AOM as a function of the frequency of the standing flexural acoustic wave. When the acoustic frequency changes, the periodicity of the perturbation also varies, and hence the phase-matching condition is shifted to a different resonant wavelength. Figure 3(a) illustrates the shift of the optical resonant wavelength as a function of the acoustic frequency. These transmission spectra were measured using a broadband light source and an optical spectrum analyzer (OSA) with 50-pm resolution. The measured spectra give the average transmission of the AOM. The three spectra reported in Fig. 3(a) correspond to three different acoustic frequencies which give rise to a transmission dip at different optical resonant wavelengths. According to the phase-matching condition, the resonant wavelength shifts to shorter wavelengths as the acoustic frequency increases. The inset of Fig. 3(a) shows a linear dependence of the resonant wavelength with the acoustic frequency f_a. The rate of change was measured to be -0.17 nm/kHz. Figure 3(a) also shows that the transmission dips have different depths as functions of f_a. This feature is quite common in this kind of acousto-optic devices, and its origin is the nonflat frequency response of the PD and the acoustic fiber resonator. For the specific device of our experiments, the highest mode-coupling was found to be around an optical wavelength of 1551 nm. Thus, in order to obtain the maximal mode-coupling, and consequently the highest modulation depth, the AOM is operated near this optical wavelength. On the other hand, we analyzed the operation of the AOM as a function of the RF voltage applied to the PD. Figure 3(b) shows the transmission spectra of the AOM at a fixed acoustic frequency and for different voltages applied to the PD. For this set of measurements, the applied voltage was varied in a range between 6 and 40 V, and the acoustic frequency was fixed at 2.3731 MHz. As it can be observed, for low voltages, the coupling and the transfer of power between the core and the cladding mode increase, resulting in a maximal attenuation notch at 18 V. Beyond this voltage the depth of the transmission dip reduces gradually since the two modes are overcoupled and the net transfer of power is reduced. In addition, the response of the PD degrades for

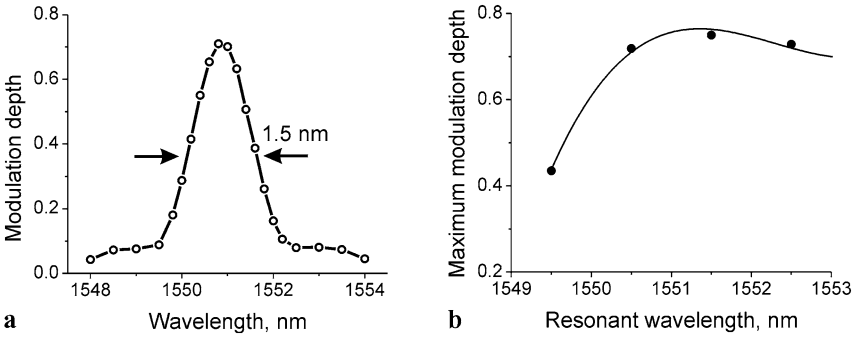

Fig. 4 (**a**) Modulation depth as a function of the optical wavelength at constant acoustic frequency (2.37315 MHz) and RF voltage (18 V). (**b**) Maximum modulation depth versus the resonant optical wavelength around 1551 nm

high voltage values due to an excessive heating. Most of our experiments were carried out using voltages around 18 V, where a stable and linear response of the PD was observed.

Finally we measured the modulation depth as a function of the optical wavelength, when both the acoustic frequency and the RF voltage were fixed. The intermodal coupling exhibits a relatively broad bandwidth around the resonant wavelength that satisfies the phase-matching condition. Figure 4(a) shows the modulation dependence around the resonant wavelength of 1551 nm when $f_a = 2.37315$ MHz and $V_{\mathrm{PD}} = 18$ V. At the resonant wavelength the modulation depth is maximal and symmetrically decreases for longer and shorter wavelengths. The measured full width at half maximum (FWHM) of the AOM is 1.5 nm, with a maximum modulation depth of 72%. Figure 4(b) shows the maximum modulation depth versus the resonant optical wavelength. This last characterization was carried out by changing slightly the RF frequency, according to the calibration reported in Fig. 3(a) and a constant voltage of 18 V.

From the point of view of the implementation of active mode-locking using this AOM, we can select certain ranges of parameters with an optimum performance of the device. Thus, the AOM can be operated with a modulation depth higher than 0.7 in the optical wavelength range 1551–1553 nm, which corresponds to the acoustic frequency range 2.3739–2.3619 MHz, using an RF voltage of ∼18 V. The AOM will exhibit low insertion loss (−0.75 dB) and relatively broad modulation bandwidth, 1.5 nm. Fine tuning of the acoustic frequency will permit a precise match of the cavity round trip time with the modulation period.

3 Experimental characterization

A schematic diagram of the mode-locked fiber ring laser is illustrated in Fig. 5. The medium gain was provided by 2.85 m of an erbium-doped fiber (EDF) containing 300 ppm Er^{3+}, with a cut-off wavelength of 939 nm, and a numerical aperture of 0.24. The active fiber was pumped through a wavelength division multiplexer coupler (WDM) by a 976-nm pigtailed laser diode, providing a maximum pump power

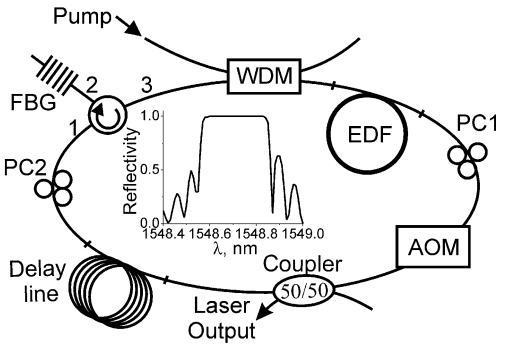

Fig. 5 Schematic setup of the mode-locked fiber ring laser. The *inset* is the reflection spectrum of the FBG

of 600 mW. Next, following a clockwise direction, the AOM was inserted, followed by a symmetrical optical coupler, and one of whose ports provided the output light pulses. The remaining port of the symmetrical coupler was connected to a delay line; this delay line was necessary in order to match the round-trip time with the modulation period. Then, port 1 of a polarization-independent three-port optical circulator (OC) was connected to the end of the delay line. The OC was used not only to force unidirectional operation within the ring cavity but to incorporate simultaneously, via port 2, a fiber Bragg grating (FBG) as a spectral filter. The FBG had a Bragg wavelength of 1548.7 nm, with a flat reflectivity near 100%, and an FWHM bandwidth of 0.3 nm. The ring cavity was closed by connecting port 3 of the OC to the WDM. Finally, two polarization controllers were added within the cavity PC1 and PC2 in order to allow a fine adjustment of the polarization.

The acoustic frequency f_a is selected to be the same as in Fig. 2, i.e., 2.37315 MHz. Thus, the frequency of modulation is two times f_a, i.e., 4.75 MHz. Assuming an effective index (n_{eff}) of 1.4457, the required cavity length, $L_{\mathrm{cavity}} = c/(n_{\mathrm{eff}} 2 f_a)$, is calculated to be 43.72 m; however, small errors in cavity length are expected, and these are compensated by a fine adjustment of the acoustic frequency. The acoustic frequency range 2.3739–2.3619 MHz allows a precise matching of the cavity length from 43.71 m to 43.93 m. Thus, in order to obtain a precise matching of the cavity

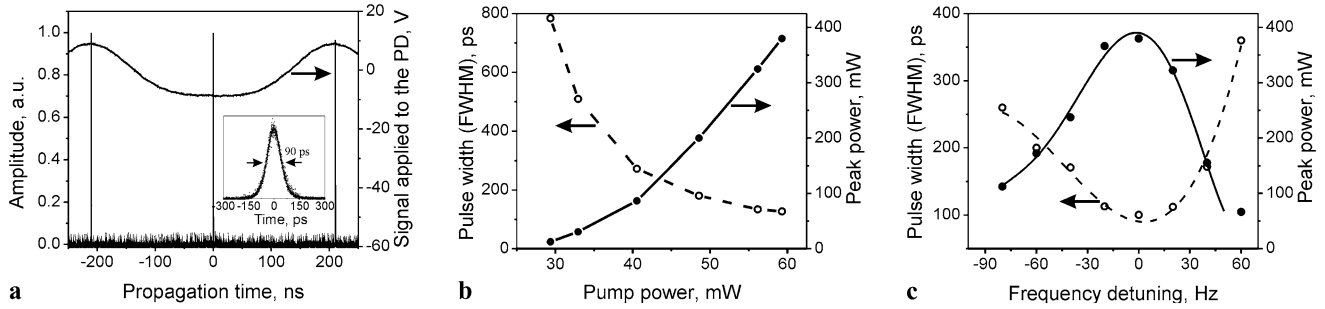

Fig. 6 (**a**) RF voltage used to drive the PD and mode-locked train of pulses generated at 4.73776 MHz with 60 mW of pump power. The *inset* shows a single pulse of 90-ps pulse width together with its corresponding fitting by a $\mathrm{sech}^2(x)$ function. (**b**) Pulse width (FWHM) and peak power of the optical pulses as functions of the pump power (*open* and *solid scatter points*, respectively). (**c**) Pulse width (FWHM) and peak powers as functions of the frequency detuning for a fixed $V_{\mathrm{PD}} = 14$ V and pump power of 60 mW

length with the acoustic frequency, errors in cavity length are compensated by adjusting the acoustic frequency, at the rate 1.84 cm/kHz ($\partial L_{\mathrm{cavity}}/\partial f_a = -L_{\mathrm{cavity}}/f_a$). Since any change of the acoustic frequency produces a shift of the optical resonant wavelength, when this is varied, the Bragg wavelength of the FBG need to be shifted to match the optical resonant wavelength of the AOM. For that reason, the FBG is mounted on a translation stage to provide wavelength tuning in a range between 1548.7 and 1552 nm. This allows a precise matching of the laser wavelength with the resonant wavelength of the AOM.

The dispersion (D) of the different sections of the laser was measured by the frequency-domain modulated-carrier method. The laser cavity is a mixed-dispersion fiber ring consisting of 2.85 m EDF with $D = -18.8$ ps/(nm km), 3.47 m SMF-28 with $D = 17.89$ ps/(nm km), 14.47 m Corning LEAF fiber with $D = 4.29$ ps/(nm km), 18.91 m Fibercore SM980 with $D = -5$ ps/(nm km), and 1.4 m OFS 980 with $D = -3.53$ ps/(nm km). The SMF-28 and OFS 980 optical fibers correspond to the pigtails of the OC and WDM, respectively, whereas the LEAF and Fibercore SM980 fibers correspond to the delay line. Thus, the average cavity dispersion results slightly anomalous with $D_{\mathrm{avg}} = 0.4$ ps/(nm km). We measured also the dispersion of the OC and WDM, and both resulted normal with a group delay per wavelength unit of -0.3 ps/nm and -0.04 ps/nm, respectively.

Mode-locking operation was obtained at the modulation frequency of 4.73776 MHz and an optical wavelength of 1551.5 nm. The RF signal used to drive the piezoelectric transducer together with the train of mode-locked pulses is shown in Fig. 6(a). For measurements of the pulse parameters, we use a sampling oscilloscope with 9-ps FWHM optical resolution. As it can be observed, the frequency of the optical pulse train is twice the frequency of the signal used to drive the PD in the modulator (2.36888 MHz). The inset shows the shortest pulse reached with this configuration. The resulting pulse has a maximum peak power of 380 mW and pulse width (FWHM) of 90 ps. The pulses were best fitted by a $\mathrm{sech}^2(x)$ function; neither Gaussian nor Lorentzian functions improved the fitting, which is an expected profile in this type of dispersion-mixed cavities [10].

If we compare the narrowest pulses obtained with this configuration (90 ps) with the narrowest pulses reported in our previous work (95 ps) [6] where the same type of AOM was used, we find nearly no difference. However, from the laser operation point of view, there is an important improvement, since the present arrangement is rather more stable, and the laser can be adjusted more easily. We attribute this improvement to the FBG used, which has a flat spectral reflectivity (see Fig. 5), making less critical the spectral matching between the FBG reflectivity with the resonant dip of the AOM. On the contrary, the FBG used in [6] was of nearly the same FWHM but with a lower reflectivity (50%). As a consequence, any spectral detuning resulted in a larger variation in reflectivity, which in turn induced a higher difficulty to stabilize the laser operation. Figure 6(b) shows the dependence of the pulse's parameters as the pump power is varied. Mode-locking operation was found in a range between 30 to 60 mW of pump power. As it can be observed, the pulse width decreases, whereas the peak power increases with the pump power. The energy of each pulse reveals that pulse energy increases from 11.13 pJ to 54.75 pJ as the pump power increases from 30 to 60 mW, respectively.

From a practical point of view, it is interesting to quantify the maximum allowable frequency detuning ($\Delta\nu$), i.e., the maximum difference between the reciprocal of the cavity round-trip time and the modulation frequency, that sustains mode locking. Figure 6(c) shows the variation of the pulse's parameters as the frequency of the RF signal applied to the PD is changed. Mode-locking of this laser permits a maximum detuning of about ± 60 Hz in any direction. The efficiency of the proposed AOM to provide high modulation depths not only helps to reach narrower pulses, but also allows a higher frequency detuning, as compared with a similar configuration with a lower modulation depth. In a certain sense, this is desirable, since it simplifies the operation of

the laser and alleviates the stability requirements on the RF source [11].

3.1 Dependence with the applied voltage to the piezoelectric

There is a direct relationship between the applied voltage to the PD and the modulation depth; although this relationship is not linear, due to the characteristic periodical behavior of the mode-coupling. In this subsection, we will show the dependence of the pulse's parameters as the modulation depth, via the applied voltage, is varied. Figure 7 gives the dependence of the pulse's parameters as functions of the RF voltage applied to the PD, in the range between 8 and 22 V. In the lower limit, an applied voltage lower than 8 V, we found that the modulation attenuation was too low to produce mode-locking, see Fig. 3(b). In Fig. 7 we can observe the narrowing of the output light pulses as the voltage increases, from 150 ps at 8 V up to 90 ps for an applied voltage of 12 V. In this range, the modulation depth increases with the applied voltage. According to mode-locking theory, the modulation depth and the pulse width are inverse parameters [12]. In this sense, this narrowing is an expected behavior. A further increment in the applied voltage from 12 V up to 22 V does not induces a further narrowing, but slightly leads to broader light pulses, because the modulation depth start to decrease again. Further narrowing by an increment in the modulation depth seems unlikely, because the modulation depth provided by the AOM is indeed very high (up to 0.74). For example, a 10% higher modulation deep, i.e., from 0.74 to 0.814, would only induce a 2% narrower pulse width, according to the known dependence of pulse width with the reciprocal of the 4th root of the modulation depth [12]. As a consequence, there is not enough margin of improvement in this specific parameter to induce a noticeable change in the pulse width.

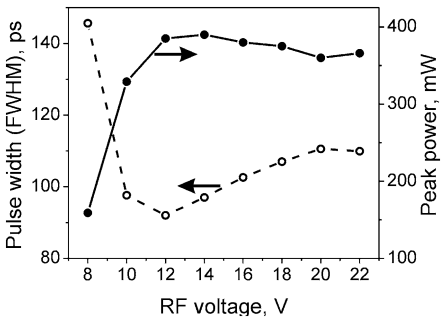

Fig. 7 Pulse width (FWHM) and peak powers versus RF voltage at $f_a = 2.36888$ MHz (*open* and *solid scatter points*, respectively). The pump power was 60 mW

3.2 Dependence with the EDF length

The dependence on the pulse parameters as a function of the EDF length is described in this section. The EDF was varied in the range 2.15 m to 4.36 m, keeping constant the cavity length, (43.7 m), by adjusting each time the length of the delay line. By changing the length of the EDF we changed not only the gain within the cavity but also the average cavity dispersion. In fact, we verified that it was possible to operate this laser in both dispersion regimes, i.e., normal and anomalous. Figure 8(a) shows the dependence of the pulse's parameters as functions of the EDF length. This figure also includes the information of the average dispersion D_{ave} for each EDF fiber length. Mode-locking operation was achieved at a minimum pump power of 345 mW, 60 mW, and 25 mW, from shorter to longer EDF fiber lengths, respectively. As the EDF length decreases, output light pulses becomes narrower. If we correlate the EDF length with the cavity gain, then this behavior for the pulse width agrees with the theoretical model developed by Kuizenga and Siegman for homogeneously broadened actively mode-locked lasers [12]. Optical pulses of 65-ps time width and 1.35-W peak power were obtained by using an EDF length of 2.15 m, which gives a dispersion average of 0.8 ps/(nm km). This result represents an improvement of 27% for the pulse width and 255% for the peak power, as compared with our initial configuration of 2.85 m of EDF length (90-ps pulse width and 380-mW peak power). Further narrowing by this trend was not possible, since no mode-locked output pulses were observed for EDF lengths shorter than 2.15 m. Figure 8(b) shows the frequency detuning for the mode-locked pulses obtained at each EDF length. As it can be observed, the detuning range reduces as the EDF decreases. This result

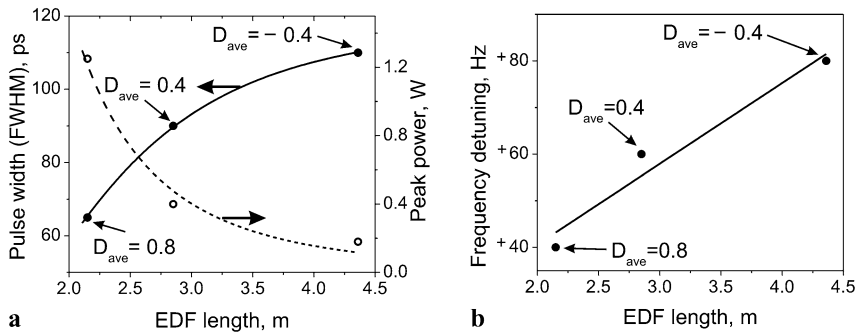

Fig. 8 (**a**) Pulse's parameters versus EDF length. (**b**) Frequency detuning versus EDF length. The label of each point gives the dispersion average

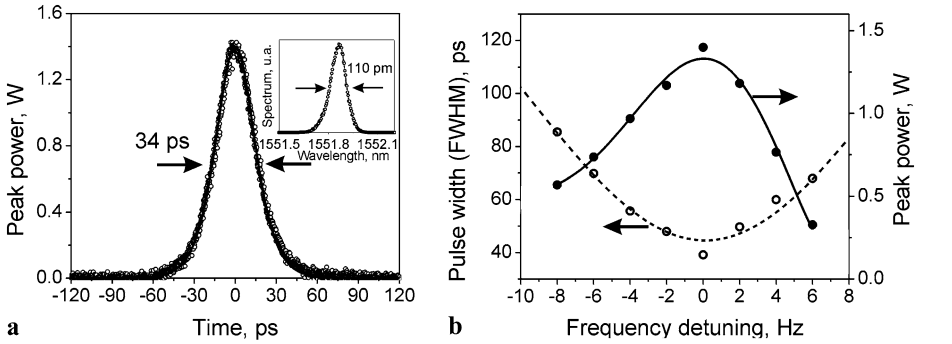

Fig. 9 (**a**) Oscilloscope trace of a single mode-locked pulse at 4.73-MHz repetition frequency. The *inset* gives the measured optical spectrum of the laser. (**b**) Pulse duration and peak power versus the frequency detuning

implies that frequency tuning is an important parameter as the mode-locked pulses become narrower. This laser permits a maximum detuning of about ±80, ±60, and ±40 Hz for the mode-locked pulses of 105, 90, and 65 ps, respectively.

3.3 Dependence with the FBG bandwidth

An important parameter of our laser arrangement is the FBG bandwidth, which acts as a spectral filter. Its bandwidth is selected narrower than the AOM bandwidth; otherwise modes not amplitude modulated would interfere in the mode-locking process. For this reason, we used first a 0.3-nm bandwidth FBG, which fulfills this requirement, since the AOM bandwidth is of 1.5 nm. However, since a larger number of modes locked—i.e. amplitude modulated—would produce narrower mode-locked pulses, we found that there was margin for improvement, since the bandwidth of the FBG used is far to be close to the AOM bandwidth. For this reason, we replace our initial FBG with another FBG, which also has a flat unit reflectivity, but a broader optical bandwidth of 0.7 nm. Figure 9 shows the shortest pulse obtained with this configuration, by using an EDF length of 2.45 m at a pump power of 265 mW. The measured temporal width was 34 ps (FWHM), with a maximum peak power of 1.4 W. For this pulse, the spectral linewidth was measured to be 110 pm (i.e., 13.7 GHz at 1551.9 nm), using a 50-pm resolution optical spectrum analyzer. On the other hand, a Fourier-transform limited $\mathrm{sech}^2(x)$ pulse should have a spectral linewidth of 9.3 GHz. From the comparison between this last value and the linewidth measurement we conclude that the optical pulses of our mode-locked laser could have some moderate degree of chirp. The soliton number N of the optical pulse, defined as the square root of the ratio between the dispersion and the nonlinear length, is estimated as 31.86 for the average cavity dispersion D_{ave} of 0.65 ps/(nm km). From this result a soliton compression effect could be expected since $N \gg 1$; however, the small degree of chirp and the $\mathrm{sech}^2(x)$ profile of the optical pulse reveal a not significant compression in the laser cavity.

As it can be observed, the spectral linewidth of the laser is rather shorter than the 0.7-nm bandwidth of the FBG. In this respect, we believe that the combination of the spectral response of the AOM (see, for example, Fig. 2(a)) with the spectral response of the FBG can establish a severe limitation to the laser linewidth. Further narrowing by this trend, i.e., by designing a broader bandwidth FBG, is theoretically possible, but experimentally challenging, because of the difficulties associated with the fabrication of a broad bandwidth FBG without chirp. Finally, we present the variation of the pulse parameters as a function of the frequency detuning for this configuration when the measured allowable frequency detuning was of ±8 Hz. According to theory of detuning in AM mode locking, the maximum allowable detuning is inversely proportional to the modulator optical bandwidth, in this case replaced by the FBG bandwidth [11]. Since the later has been increased noticeably, i.e., from 0.3 nm to 0.7 nm, a reduction in the allowable detuning is an expected result.

4 Conclusions

In this work we have carried out an experimental characterization of an actively mode-locked all-fiber ring laser based on a recently developed amplitude modulator. First, we have presented a detailed characterization of the modulator itself. Then, the pulse duration, the peak power, and the frequency detuning have been characterized for different cavity configurations. Thus, the optimization of the laser cavity has led to a stable operation of the laser with pulses of 34-ps time duration and 1.4-W peak power at a repetition rate of 4.7 MHz. The implementation of a theoretical simulation of the laser will contribute to identify which cavity parameters are at present limiting the effective optical bandwidth of the laser and, consequently, any further reduction of the pulse duration.

Acknowledgements This work has been financially supported by the *Ministerio de Educación y Ciencia and the Generalitat Valenciana of Spain* (projects TEC2008-05490 and PROMETEO/2009/077, respectively). M. Bello-Jiménez was supported by *CONACyT* (Mexican Council for Science and Technology). C. Cuadrado-Laborde acknowledges the *Programa de Investigadores Invitados de la Universidad de Valencia (Spain)*.

References

1. M.W. Phillips, A.I. Ferguson, G.S. Kino, D.B. Patterson, Opt. Lett. **14**, 680 (1989)
2. D.O. Culverhouse, D.J. Richardson, T.A. Birks, P.St.J. Russel, Opt. Lett. **20**, 2381 (1995)
3. M.Y. Jeon, H.K. Lee, K.H. Kim, E.H. Lee, W.Y. Oh, B.Y. Kim, H.W. Lee, Y.W. Koh, Opt. Commun. **149**, 312 (1998)
4. N. Myrén, W. Margulis, IEEE Photonics Technol. Lett. **17**, 2047 (2005)
5. C. Cuadrado-Laborde, A. Díez, M. Delgado-Pinar, J.L. Cruz, M.V. Andrés, Opt. Lett. **34**, 1111 (2009)
6. M. Bello-Jiménez, C. Cuadrado-Laborde, D. Sáez-Rodriguez, A. Díez, J.L. Cruz, M.V. Andrés, Opt. Lett. **35**, 1 (2010)
7. B.Y. Kim, J.N. Blake, H.E. Engan, H.J. Shaw, Opt. Lett. **11**, 389 (1986)
8. T.A. Birks, P.St. Russell, D.O. Culverhouse, J. Lightwave Technol. **14**, 2519 (1996)
9. F. Abrishamian, S. Nagai, S. Sato, M. Imai, Opt. Quantum Electron. **40**, 665 (2008)
10. P. Bélanger, Opt. Express **13**, 8089 (2005)
11. Y. Li, C. Lou, M. Han, Y. Gao, Opt. Quantum Electron. **33**, 589 (2001)
12. D.J. Kuizenga, A.E. Siegman, IEEE J. Quantum Electron. **QE-6**, 694 (1970)